Uncertainties of inherent optical properties obtained from semianalytical inversions of ocean color

Peng Wang, Emmanuel S. Boss, and Collin Roesler

We present a method to quantify the uncertainties in the in-water constituent absorption and backscattering coefficients obtained from an inversion of remotely sensed reflectance (r_{rs}). We first find a set of positive inversion solutions within a given uncertainty range around the values of the inverted r_{rs}. The uncertainties of the solutions are then computed based on the statistics of these solutions. We demonstrate the uncertainty calculation algorithm using a specific semianalytic inversion model applied to both a field and a simulated data set. When the associated uncertainties are taken into account, the inverted parameters are generally within the uncertainties of the measured (or simulated) parameters, highlighting the success of the inversion and the method to obtain uncertainties. The specific inversion we use, however, fails to retrieve two spectral parameters within a usable range. The method presented is general and can be applied to all existing semianalytical inversion algorithms. © 2005 Optical Society of America

OCIS codes: 010.4450, 280.0280.

1. Introduction

The inherent optical properties (IOPs; the optical properties that are independent of the ambient light field[1]) with appropriate boundary conditions, determine the Sun-illuminated aquatic light field. IOPs include the absorption and backscattering coefficients. The apparent optical properties[1] (AOPs) are connected to the IOPs by the equation of radiative transfer.[1–2] Approximations to the radiative transfer equation (RTE) indicate that remotely sensed reflectance (r_{rs}, also referred to as ocean color, an AOP, see notations in Table 3 for symbols and definitions used in this paper) depends to first order on the absorption and backscattering coefficients.[3–4] One goal in using ocean color inversions is to obtain the absorption and backscattering coefficients due to different in-water constituents by inverting r_{rs}. The three main components of IOPs that are currently retrievable are phytoplankton absorption, combined absorption of colored dissolved organic matter (CDOM) and nonalgal particles (NAP), and particulate backscattering.

Obtaining these IOPs is of importance as they relate to standing stocks and rate processes of important aquatic carbon pools.[5–8]

Semianalytical ocean-color inversion algorithms[9–13] are based on approximate solutions to the RTE (the analytical part) and assumptions regarding the spectral shapes of IOPs (the empirical part). Unlike purely empirical algorithms, semianalytical algorithms are not limited to certain geographical regions or water type.

Currently, no accepted method exists for quantifying the uncertainties associated with the inversion products of semianalytical models, and their output has been reported without the associated error bars. Some general confidence intervals (e.g., not associated with each inverted r_{rs}) have been estimated on the basis of sensitivity analysis on a subset of the data[9,11–12] or the basis of the magnitude of residuals between the measured spectra and that constructed from the inverted IOPs.[14] Without an estimate of the uncertainties in inversion products (e.g., IOPs) it is impossible either to propagate errors when inversion products are used as inputs into primary production and carbon models or to assess whether closure between remotely sensed estimates of IOPs and in-water IOPs has been achieved. In this paper we present a procedure to obtain uncertainty estimates for inverted IOPs obtained by semianalytical inversions.

P. Wang and E. S. Boss (emmanuel.boss@maine.edu) are with the University of Maine, 5741 Libby Hall, Orono, Maine 04469-5741. C. Roesler is with the Bigelow Laboratory for Ocean Sciences, P.O. Box 475, West Boothbay Harbor, Maine 04575-0475.

2. Data and Methods

A. Data Sets

1. Simulated Data Set

We demonstrate our approach using a synthetic data set developed by Z. P. Lee[15] as part of the activities of the International Ocean Color Coordination Group (IOCCG) Ocean-Color Algorithms coordinating group.[16] This data set contains both spectral IOPs based on observations and theoretical analysis of field data and the corresponding r_{rs} derived from the IOPs in which a radiative transfer model (Hydrolight, Sequoia Scientific) for a Sun at 30° zenith angle was used. In total, there are 500 IOP and r_{rs} spectra in the synthetic data set that are freely available on the WWW.[17] Wavelengths used for inversion of simulated data vary from 400 to 650 nm with a 10-nm interval (number of wavelength, $m = 26$). We assume the IOPs of the simulated data set to be error free.

2. Field Data Set

The field data set was collected during the summers of 2000 and 2001 as part of the Hyperspectral Coupled Ocean Dynamics Experiments (HyCODE) field experiment at the Mid-Atlantic Bight in the vicinity of the Long-term Ecological Observatory site (LEO-15) off the coast of New Jersey in water depths of less than 25 m.[18]

Radiometric quantities were collected with a Satlantic, Inc. HyperTSRB (Tethered Spectral Radiometer Buoy) that measured upwelling radiance at 0.66 m below the sea surface, $L_u(\lambda, 0.66 \text{ m})$, and downwelling irradiance just above the sea surface, $E_d(\lambda, 0^+ \text{ m})$ between wavelengths of 400 and 800 nm at 1-nm resolution. To avoid the chlorophyll fluorescence contribution near 680 nm, only r_{rs} between wavelengths of 412 and 650 nm are used as input for the inversion preformed in the current paper (number of wavelengths, $m = 239$). Here we use a total of 31 independent IOP-r_{rs} match-up stations. A subset (year 2000) of these data (IOP and r_{rs}) was used in previous studies.[18,19]

IOPs were measured with a free-falling slow descent rate optics platform (Slowdrop[20]). Absorption by dissolved and particulate materials and backscattering data were collected with 2 WETLabs ac-9s (one ac-9 with a 0.2-μm prefilter, the other unfiltered) and a HOBILab Hydroscat-6, respectively. Data were collected and processed according to standard protocols.[21] At each station the IOPs were collected as a series of consecutive vertical profiles. For match-up IOPs we chose the IOPs profile with least variability from the surface down to a depth equal to (absorption)$^{-1}$, from which approximately 90% of the signal emanates.[22] For that profile the difference between maximum and minimum values is used to quantify the uncertainty in the observed IOP with the median being the expected value.

We use a simple analytical model for converting the radiance as measured by a TSRB to water-leaving radiance.[23] Above-surface remote-sensing reflectance, R_{rs}, is then computed with the following relation:

$$R_{rs} = \frac{L_w(\lambda, \ 0^+)}{E_d(\lambda, \ 0^+)} = C(\lambda) \frac{L_w(\lambda, \ 0.66m)}{E_d(\lambda, \ 0^+)},$$

$$C(\lambda) = \frac{t}{n^2} \exp[0.66 k_L(\lambda)], \tag{1}$$

where the diffuse attenuation k_L is approximated by $a(\lambda)/\cos\theta_s$, $a(\lambda)$ is the absorption coefficient, $n \approx 1.34$ is the index of refraction of seawater, $t \approx 0.98$ is the radiance transmittance across the air–water interface, and θ_s is the in-water solar zenith angle. We convert above-surface remote-sensing reflectance spectra R_{rs} to below-surface spectra using a relation from Lee et al.[24]:

$$r_{rs} = \frac{R_{rs}}{0.52 + 1.7 * R_{rs}}. \tag{2}$$

B. Inversion Model

Semianalytical IOP inversion models[9–12] are based on three assumptions.

The relation between r_{rs} and the absorption and backscattering coefficients is known.

The absorption and backscattering coefficients for pure seawater are known.

The spectral shapes of the absorption and backscattering coefficients for in-water constituents are known.

These models often vary in their choice of the r_{rs}–IOPs relation, the assumed spectral shape of the component IOPs, the wavelength range used in the inversion, and the specifics of the mathematical method of inversion. Below is the description of the specific model used in this paper.

1. Relation between r_{rs} and Inherent Optical Properties

The relation between $r_{rs}(\lambda)$ and the backscattering to absorption coefficients is approximated by[25]

$$r_{rs}(\lambda) = \frac{L_u(\lambda, \ 0^-)}{E_d(\lambda, \ 0^-)}$$

$$\cong 0.0949 \frac{b_b(\lambda)}{a(\lambda) + b_b(\lambda)} + 0.0794 \left(\frac{b_b(\lambda)}{a(\lambda) + b_b(\lambda)} \right)^2, \tag{3}$$

where $L_u(\lambda, 0^-)$ and $E_d(\lambda, 0^-)$ are the upwelling radiance and downwelling irradiance just beneath the sea surface. The quadratic term is significant ($>4\%$) when $b_b/(a + b_b) > 0.2$, for example, in extremely turbid waters in green wavelengths.

2. Assumed Spectral Shapes of the Constituent Inherent Optical Properties

The total absorption coefficient is partitioned as follows:

$$a(\lambda) = a_{\mathrm{sw}}(\lambda) + a_{\mathrm{ph}}(\lambda) + a_{\mathrm{CDOM+NAP}}(\lambda), \quad (4)$$

where the subscripts sw, ph, and CDOM + NAP designate seawater, phytoplankton and the combined contribution of CDOM and NAP. CDOM and NAP absorption is not separated owing to the similarities in their spectral shapes.[9,12] The spectral absorption coefficient $a_{\mathrm{sw}}(\lambda)$ for seawater is computed for a given salinity and temperature.[26,27]

The spectral absorption coefficient of phytoplankton, $a_{\mathrm{ph}}(\lambda)$, is parameterized as a function of a size parameter describing the relative contributions of two spectral shapes associated with picophytoplankton and microphytoplankton[28]:

$$a_{\mathrm{ph}}(\lambda) = a_{\mathrm{ph}}(\lambda_0)[S_f a_{\mathrm{pico}}(\lambda) + (1 - S_f)a_{\mathrm{micro}}(\lambda)], \quad (5)$$

where $a_{\mathrm{pico}}(\lambda)$ and $a_{\mathrm{micro}}(\lambda)$ are the shapes corresponding to the normalized absorption spectral for the smallest and largest cells (values provided in Ciotti *et al.*[28]), λ_0 is the reference wavelength, and the size parameter S_f varies between zero and one. We chose this parameterization of a_{ph} based on the success of Ciotti *et al.*[28] in fitting spectra of a_{ph} measured in a wide range of natural waters.

The spectral dependence of the combined absorption by CDOM and NAP is assumed to be

$$a_{\mathrm{CDOM+NAP}}(\lambda) = a_{\mathrm{CDOM+NAP}}(\lambda_0)\exp[-S(\lambda - \lambda_0)], \quad (6)$$

where S is the combined CDOM and NAP spectral slope. This function has been found to be an adequate representation of observed CDOM and NAP[29,30] with S ranging between 0.008 and 0.023.

The total backscattering coefficient, $b_b(\lambda)$, is approximated by

$$b_b(\lambda) = b_{b\mathrm{sw}}(\lambda) + b_{b\mathrm{p}}(\lambda), \quad (7)$$

where the subscripts sw and p represent water and particulate backscattering, respectively. The spectral backscattering coefficient $b_{b\mathrm{sw}}(\lambda)$ for seawater is computed for a given salinity.[31–32]

The spectral particle backscattering coefficient is assumed to obey

$$b_{b\mathrm{p}}(\lambda) = b_{b\mathrm{p}}(\lambda_0)(\lambda/\lambda_0)^{-Y}, \quad (8)$$

consistent with many previous studies,[9–12] though without in-water validation.[33,34]

To account for variability in space and time of the spectral shapes of the IOP we perform the r_{rs} inversion allowing the shape parameters (S_f for phytoplankton absorption, spectral slope S for the combined absorption by CDOM and NAP and spec-

tral slope Y for the particulate backscattering) to vary within most of their observed range of variability ($0 \leq S_f \leq 1$, $0.01 \leq S \leq 0.02$, $0 \leq Y \leq 2$). For each parameter we use 11 different values with equal intervals between their maximum and minimum, resulting in $11^3 = 1331$ different inversion computations for each r_{rs} spanning all the possible combinations of the shape parameters.

3. Inversion Technique

Following Hoge and Lyon,[11] we define

$$X \equiv \frac{b_b}{a + b_b} \rightarrow a + b_b\left(1 - \frac{1}{X}\right) = 0, \quad (9)$$

where X is computed as the one positive quadratic solution of Eq. (3). Denoting $v \equiv 1 - 1/X$ and separating the known seawater IOP, we obtain an equation for the unknown IOPs at each wavelength λ_i, where $i = 1, \ldots m$ (m is the number of wavelengths):

$$a_{\mathrm{ph}}(\lambda_i) + a_{\mathrm{CDOM+NAP}}(\lambda_i) + b_{b\mathrm{p}}(\lambda_i)v(\lambda_i) = -[a_{\mathrm{sw}}(\lambda_i) + b_{bsw}(\lambda_i)v(\lambda_i)]. \quad (10)$$

With the known right-hand side (RHS) denoted as $h(\lambda_i) \equiv -[a_{\mathrm{sw}}(\lambda_i) + b_{bsw}(\lambda_i)v(\lambda_i)]$, Eq. (10) becomes

$$a_{\mathrm{ph}}(\lambda_i) + a_{\mathrm{CDOM+NAP}}(\lambda_i) + b_{b\mathrm{p}}(\lambda_i)v(\lambda_i) = h(\lambda_i). \quad (11)$$

Equation (11) contains three unknowns for each spectral radiance measurement. The substitution of Eqs. (5)–(7) into (11) yields

$$a_{\mathrm{ph}}(\lambda_0)[S_f a_{\mathrm{pico}}(\lambda_i) + (1 - S_f)a_{\mathrm{micro}}(\lambda_i)] + a_{\mathrm{CDOM+NAP}}(\lambda_0)\exp[-S(\lambda_i - \lambda_0)] + v(\lambda_i)b_{b\mathrm{p}}(\lambda_0)(\lambda_i/\lambda_0)^{-Y} = h(\lambda_i). \quad (12)$$

Equation (12) contains six unknowns for each wavelength; three amplitudes $a_{\mathrm{ph}}(\lambda_0)$, $a_{\mathrm{CDOM+NAP}}(\lambda_0)$, $b_{b\mathrm{p}}(\lambda_0)$ and three spectral shape parameters: S_f, S, and Y (which are not solved for but assumed for each inversion). For each choice of the spectral shape parameters we solve Eq. (12) by matrix inversion to obtain $a_{\mathrm{ph}}(\lambda_0)$, $a_{\mathrm{CDOM+NAP}}(\lambda_0)$, and $b_{b\mathrm{p}}(\lambda_0)$. A basic difference between our method compared with that of Hoge and Lyon's[11] is that in the current study we solve Eq. (12) using more wavelengths than unknowns. This makes Eq. (12) an overconstrained system for which the solution is the best solution in a least-squares sense.[35]

C. Criteria for Selection of Acceptable Solutions

For each measured r_{rs}, Eq. (12) is solved with a different combination of S_f, S, and Y, resulting in 1331 solutions. We select acceptable solutions by one, requiring that the values of all the amplitudes be positive or zero, and two, requiring that the difference between the r_{rs} constructed from the solution and the r_{rs} measured is constrained. Here we chose this constraint to be that the relative difference is less than
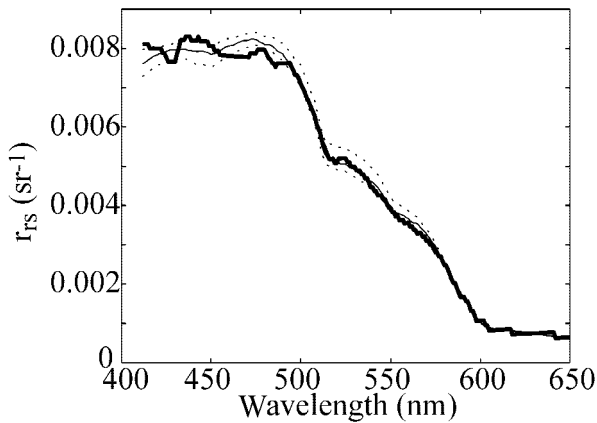
Fig. 1. Comparison of a measured r_{rs} (7/23/2001, bold curve) with the median values of all the inversion solutions (526) for which the reconstructed r_{rs} is within 10% of the measured r_{rs} at all wavelengths (thin line) and the 5th and 95th percentiles of those solutions (dotted curves).

10% at all wavelengths. This constraint is based on an analysis of the following uncertainties:

Uncertainties in the measured r_{rs} due to instrumental drift. All radiometers were field-calibrated at least every 3 days against a stable light source. The drifts in the measured radiometric quantities were found to be less than 3% for both the irradiance and the radiance sensors.[18]

Uncertainties caused by the assumed relation between r_{rs} and IOPs [Eq. (3)]. To evaluate this uncertainty, we input the locally measured IOPs into Eq. (3) and compared with the measured (or Hydrolight derived) r_{rs} for the field and simulated data set, respectively. The median relative difference for the simulated data set varies from 2.66% to 9.98% at all the wavelengths with the difference increasing from blue to red and is less than 8% for all the IOP bands measured *in situ* (not shown).

Uncertainties caused by the assumed shape of IOPs. To assess the uncertainties caused by the chosen IOP shapes, we calculate how well the assumed spectral shape fit the input data. The uncertainty of a given IOP shape is quantified by a cost function:

$$\varepsilon = \frac{1}{N}\left[\sum_{i=1}^{N}\left(\frac{\text{input} - \text{fit}}{\text{input}}\right)^2\right]^{1/2}. \quad (13)$$

We find that for 75% of the $a_{\text{CDOM+NAP}}$ and all the b_{bp} data, $\varepsilon < 0.01$. For a_{ph}, only 3% of the data has $\varepsilon < 0.01$. However, for 98.2% of a_{ph} and 100% of $a_{\text{CDOM+NAP}}$ and b_{bp}, $\varepsilon < 0.1$. The median value of the relative difference between fit and observed or assumed b_{bp} and $a_{\text{CDOM+NAP}}$ in all wavelengths is less than 4%, whereas it varies from 3% to 20.7% for a_{ph}. The largest relative differences in a_{ph} are in the red part of the spectra ($\lambda > 570$ nm), where the signal is smallest.

On the basis of the above discussion we choose a criterion for acceptance of an inversion solution if the reconstructed r_{rs} from the inverted IOPs was within 10% of the measured r_{rs} at all wavelengths (see Fig. 2 for a schematic of the algorithm) and had positive IOP amplitudes. Each acceptable solution has a corresponding set of IOP amplitudes $[a_{\text{plh}}(\lambda_0),$ $a_{\text{CDOM+NAP}}(\lambda_0), b_{bp}(\lambda_0)]$ and spectral shape parameters (S, S_f, Y). An example of a family of solutions is provided in Fig. 1. For the hundreds of solutions that are within the acceptance criterion, we calculate the median and the 5 and 95 percentiles of the amplitude and shape parameters to provide an estimate of the most likely solution, and to quantify the uncertainty of this solution (see Fig. 3 for an example of a histogram of amplitude distribution for all acceptable solutions). We refer to the 90% confidence interval as the interval separating the 5 and 95 percentiles (Table 1). In a few cases (4% of the simulated data set and 11% for the *in situ* data set) no solution was found that was within the chosen acceptance criterion, which means that no solution was found for which the reconstructed r_{rs} was within 10% of the input r_{rs} at all wavelengths or that the solution found has negative IOP amplitudes. Such cases may occur owing to larger errors resulting from errors in the input r_{rs}, in our inversion model (IOPs–r_{rs} relation and/or IOP shapes), or in both. These cases are not discussed further.

3. Results and Discussion

To compare with other published inversion algorithms and for the sake of brevity, we primarily discuss the inversion results at 410, 440, and 490 nm for absorption and 550 nm for backscattering (555 nm for the *in situ* data set). We denote by $a_{\text{p+CDOM}}$ the sum of particulate and dissolved absorptions, $a_{\text{ph}} + a_{\text{NAP+CDOM}}$. We refer to the outputs of the inversion model as 'inverted' even when obtaining the shape factors (S_f, S, and Y) that are assumed in the inversion. We provide a wide range of realistic values for these parameters and provide the statistics of these parameters from all possible solutions, a procedure similar to inversions in which the output is constrained.

A. Simulated Data Set

Comparing the optical properties between those derived from the inversion and those used to compute r_{rs} suggests that the inversion scheme is successful (Fig. 4). Both the high linear correlations and the low median relative and absolute difference show that the inverted $a_{\text{pg}}(410, 440, 490)$ and $b_{bp}(550)$ match their input values well (Table 2). For example, for the entire data set $[0.01 < a_{p+\text{CDOM}}(440) < 3.17$ m$^{-1}]$, the correlation coefficient for $a_{p+\text{CDOM}}(440)$ is 0.99, and the median relative and absolute differences are 7.75% and 0.014 m^{-1}, respectively. The correlation coefficient is 0.99 for $b_{bp}(550)$, 0.99 for $a_{\text{NAP+CDOM}}(440)$, 0.94 for $a_{\text{ph}}(440)$. Absorptions by phytoplankton and by CDOM and NAP are well retrieved. The median of the relative difference is 20% and 14% higher com-
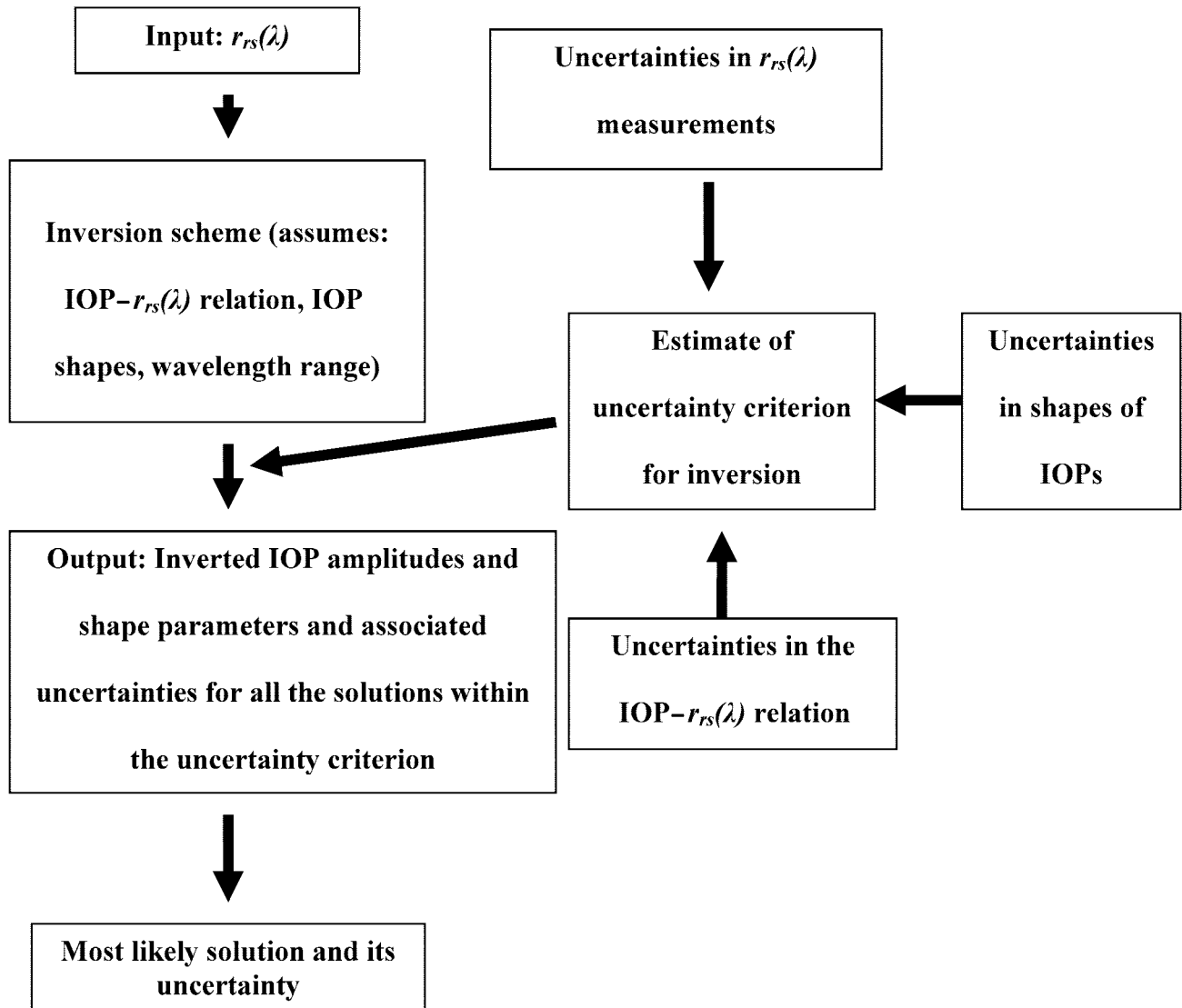
Fig. 2. Schematic flow chart of the inversion scheme and determination of the uncertainty in the inverted parameters.

pared with their total combined absorption. This is likely because both have spectral shapes that generally decrease from blue to red and thus are hard to separate.

The total absorption at 440 nm is found with fewer than 18% of the point outside the 90% confidence intervals, 43% for backscattering, 10% for absorption by dissolved materials, and 20% for absorption by phytoplankton. The percentage of input values covered by the uncertainty range is high except for the backscattering coefficients (Table 2).

The relative difference among the inverted $a_{\mathrm{CDOM+NAP}}$, a_{ph}, and b_{bp} and their input values at all wavelengths were also calculated (not shown). The inverted $a_{\mathrm{CDOM+NAP}}$ and a_{ph} values fit their input values better in the blue wavelengths; the $a_{\mathrm{CDOM+NAP}}$ percentage of the relative difference smaller than 10 is nearly 40% from 400 to 550 nm, and nearly 30% for a_{ph} from 400 to 490 nm. That percentage decreases with increasing wavelengths (7.5% for $a_{\mathrm{CDOM+NAP}}$ and

7.9% for a_{ph} at 650 nm) as signals decrease. For b_{bp}, the inverted results fit best in the middle wavelength at 490–530 nm (more than 75% have a relative difference less than 10%).

Relative magnitude of uncertainties in absorption by phytoplankton and by CDOM+NAP and backscattering by particles is relatively uniform as a function of amplitude (Fig. 4), suggesting that the algorithm used here can be used with the same degree of success within waters of high chlorophyll, CDOM, or both as well as in relatively clear waters.

Comparison of spectral shape parameters suggest that they are harder to invert than the amplitudes, in particular because of their limited dynamic range. Both medians of the inverted S and Y values are overestimated [Figs. 5(a) and 5(b)]. The correlation coefficients are high especially given the low dynamic range of these parameters ($r = 0.8$ for S and $r = 0.9$ for Y; the median of the relative difference for S and Y is 0.17 and 0.37, respectively).
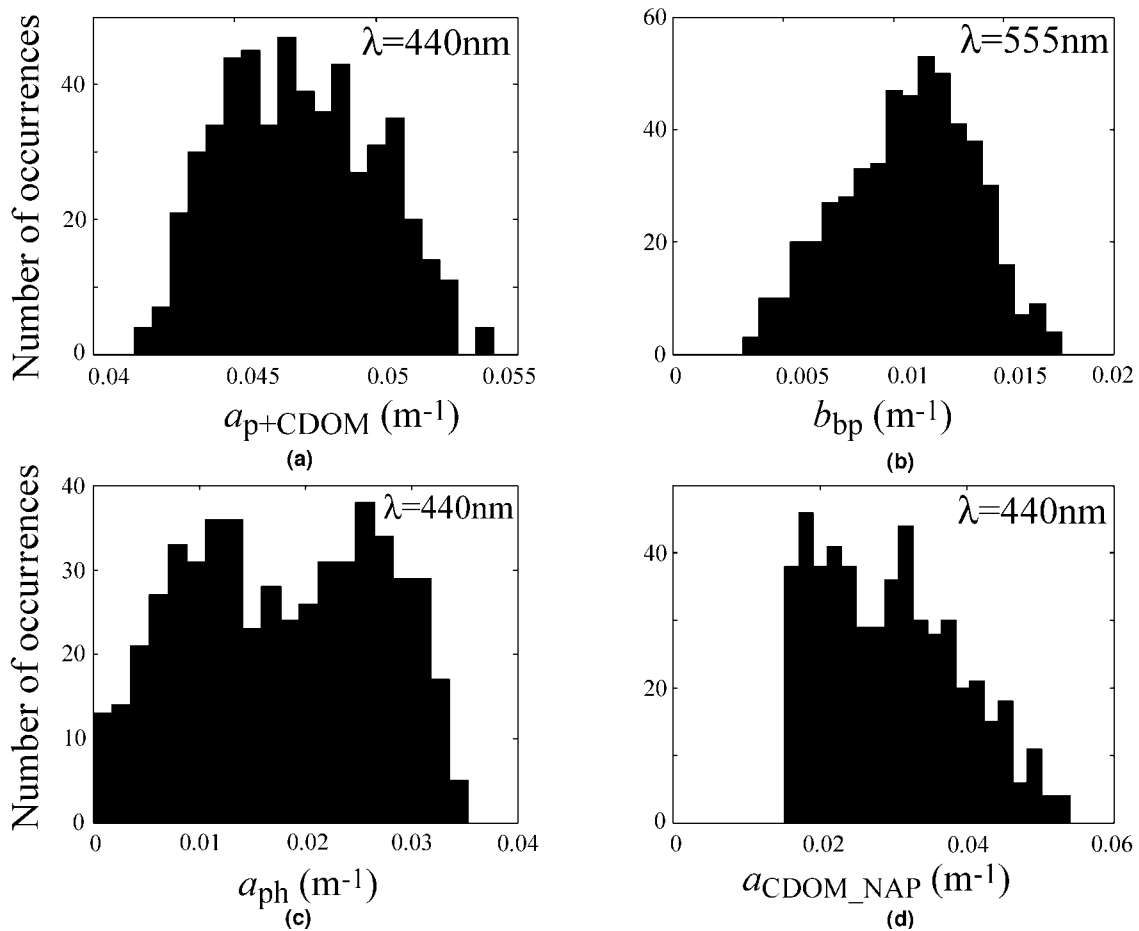
Fig. 3. Histograms of (a) the inverted total absorption coefficient ($a_{p+CDOM} = a_{ph} + a_{CDOM+NAP}$) at 440 nm , (b) the particulate backscattering coefficient (b_{bp}) at 555 nm, (c) the phytoplankton absorption coefficient (a_{ph}) at 440 nm , (d) the CDOM and NAP absorption coefficient ($a_{CDOM+NAP}$) at 440 nm for the r_{rs} presented in Fig. 1.

Inversion uncertainties are high, indicating the inability to obtain these shape parameters with high certainty.

For the phytoplankton absorption, we attempt to correlate the size factor (S_f) with the blue/red ratio of phytoplankton absorption, since size and pigment packaging are correlated.[36,37] The correlation between the size factor (S_f) for phytoplankton and the ratio of a_{ph} at 440 to 680 nm [Fig. 5(c)] is low (r = 0.18), indicating that the attempt to relate the phytoplankton size factor with the blue-to-red phytoplankton absorption ratio is not successful. Given that the input a_{ph} was not well represented by the model a_{ph} (see Subsection 2.C) it may not be surprising that the spectral shape is not retrieved well.

Table 1. Comparison between the Inverted and the Input IOP Values of the Simulated Data Set

| Compared Quantity	Dynamic Range (m^{-1})	Median Relative Difference (%)	95% Relative Difference (%)	Median Absolute Difference (m^{-1})	95% Absolute Difference (m^{-1})	R	Percentage of the Data Inside 90% Confidence Interval
a_p+CDOM(410)	0.0095 ~ 4.53	8.95	37.9	0.0194	0.671	0.988	82.9
a_p+CDOM(440)	0.0095 ~ 3.17	7.75	30.9	0.0138	0.438	0.989	83.1
a_p+CDOM(490)	0.0051 ~ 1.92	6.78	21.8	0.0047	0.157	0.992	85.8
b_{bp}(550)	0.00052 ~ 0.13	7.55	15.9	0.0006	0.0082	0.993	56.8
a_{ph}(410)	0.0034 ~ 0.42	20.5	63.4	0.0068	0.0977	0.911	84.8
a_{ph}(440)	0.0056 ~ 0.42	19.8	61.2	0.0092	0.134	0.937	80.6
a_{ph}(490)	0.0031 ~ 0.32	22.1	66.4	0.0064	0.0829	0.946	87.7
$a_{CDOM+NAP}$(410)	0.0060 ~ 4.17	14.5	43.9	0.0218	0.628	0.988	81.8
$a_{CDOM+NAP}$(440)	0.0039 ~ 2.75	14.4	40.1	0.0119	0.330	0.99	90.0
$a_{CDOM+NAP}$(490)	0.0012 ~ 1.63	14.7	61.1	0.0077	0.0939	0.991	89.1
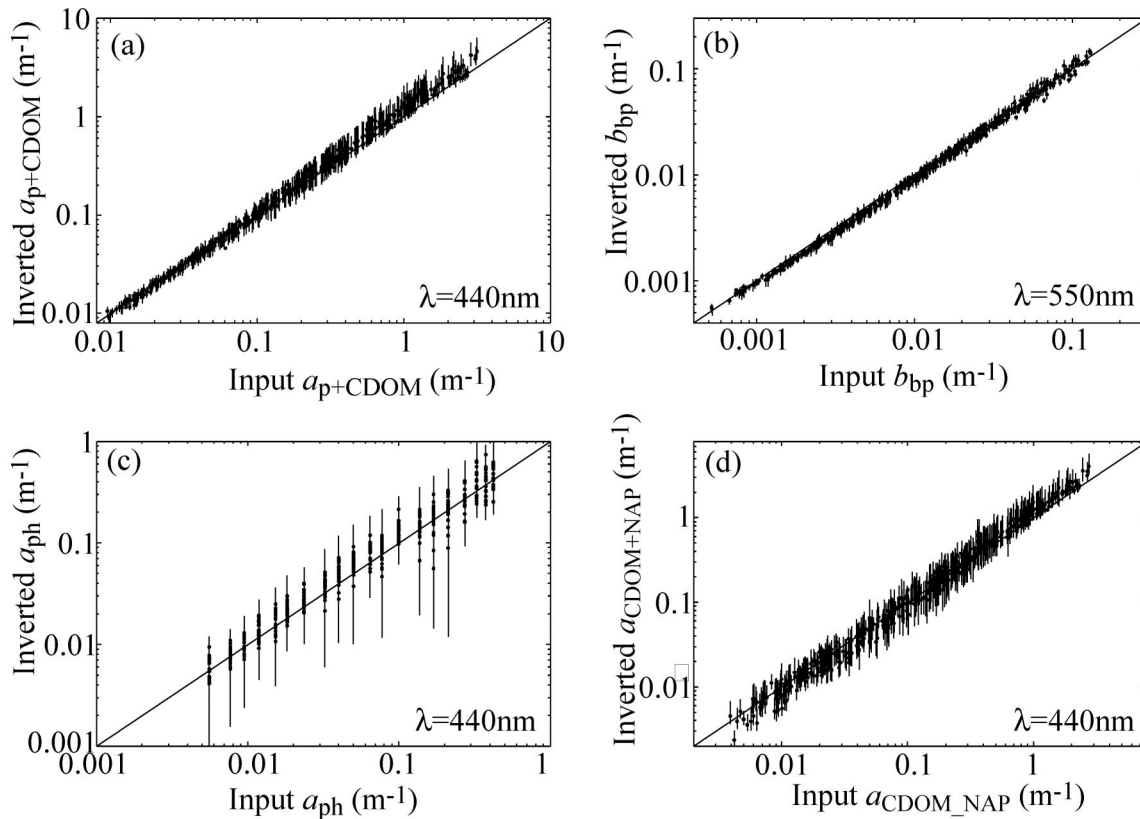
Fig. 4. Comparison of the inverted values of (a) $a_{p+\text{CDOM}}(440)$, (b) $b_{bp}(550)$, (c) $a_{ph}(440)$, (d) $a_{\text{CDOM+NAP}}(440)$ relative to the input values (x axis) for the simulated data set. Dots denote the median inverted values, whereas the lines denote the 90% confidence interval.

B. Field Data

Comparison of retrieved optical properties with those measured *in situ* at 410, 440, and 490 nm indicate good agreement (Fig. 6). Over the entire data set [$0.049 < a_{p+\text{CDOM}}(440) < 0.828$ m^{-1}, $0.001 < b_{bp}(555) < 0.0343$ m^{-1}], the correlation coefficient for $a_{p+\text{CDOM}}(440)$ is $r = 0.94$ and the median relative and absolute differences are 12% and 0.0488 m^{-1}, respectively. The correlation coefficient of $b_{bp}(555)$ is 0.98, and the median relative and absolute differences are 23% and 0.0026 m^{-1}, respectively. Note that measured IOPs are not error free (indicated by horizontal lines in Fig. 6). The particulate and dissolved absorption coefficient ($a_{p+\text{CDOM}}$) at 440 nm is

found with less than 15% of the point outside the 90% confidence interval, 65% for backscattering coefficient (b_{bp}) at 555 nm (Fig. 6).

In the *in situ* data set, the combined absorption by CDOM and NAP is unavailable. Only CDOM absorption was measured, so we compare $a_{\text{CDOM+NAP}}$ with a_{CDOM} [Fig. 6(c)]. The linear correlation coefficient for $a_{\text{CDOM+NAP}}(440)$ and $a_{\text{CDOM}}(440)$ is $r = 0.86$, and the median relative and absolute differences are 18% and 0.0368 m^{-1}, respectively. Absorption by CDOM and NAP at 440 nm is found with less than 7% of the points outside the 90% confidence interval. Not surprisingly, 73% of inverted $a_{\text{CDOM+NAP}}$ values (averaged over the three wavelengths) are higher than the mea-

Table 2. Comparison between the Inverted and the Input IOP Values of the *In Situ* Data Set

Compared Quantity Inversion/ Observation	Dynamic Range (m^{-1})	Median Relative Difference (%)	95% Relative Difference (%)	Median Absolute Difference (m^{-1})	95% Absolute Difference (m^{-1})	R	Percentage of the Point Inside 90% Confidence Interval
$a_p+\text{CDOM}(412)$	$0.047 \sim 1.01$	13.3	32.8	0.0725	0.266	0.909	85
$a_p+\text{CDOM}(440)$	$0.049 \sim 0.83$	11.7	27.9	0.0488	0.175	0.942	87.5
$a_p+\text{CDOM}(488)$	$0.025 \sim 0.49$	13.1	27.6	0.0347	0.107	0.958	80
$b_{bp}(555)$	$0.001 \sim 0.034$	22.8	36.6	0.0026	0.0085	0.975	35.5
$a_{ph}(676)$	$0.0041 \sim 0.15$	14.7	145	0.0124	0.0478	0.901	87.1
$a_{dg}(412)/a_g(412)$	$0.029 \sim 0.42$	17.6	55.3	0.0573	0.208	0.934	90.3
$a_{dg}(440)/a_g(440)$	$0.023 \sim 0.42$	17.8	48.2	0.0368	0.133	0.855	93.5
$a_{dg}(488)/a_g(488)$	$0.0095 \sim 0.14$	27.9	63.4	0.0204	0.786	0.923	93.5

Table 3. Notation

Variable	Units[a]	Definition
a	m^{-1}	Total absorption coefficient: $a_{\mathrm{sw}} + a_{\mathrm{p+CDOM}}$
a_{sw}	m^{-1}	Ocean water absorption coefficient
$a_{\mathrm{p+CDOM}}$	m^{-1}	Particulate (phytoplankton+ NAP) and CDOM absorption coefficient
$a_{\mathrm{CDOM+NAP}}$	m^{-1}	CDOM + NAP absorption coefficient
a_{ph}	m^{-1}	Phytoplankton pigments absorption coefficient
b_b	m^{-1}	Total backscattering coefficient: $b_{bsw} + b_{bp}$
b_{bsw}	m^{-1}	Ocean water backscattering coefficient
$b_{b\mathrm{p}}$	m^{-1}	Particulate backscattering
S	nm^{-1}	Combined CDOM and NAP spectral slope
S_f		Phytoplankton size parameter
Y		Particulate backscattering spectral slope
a_{pico}	m^{2}mg^{-1}	Phytoplankton absorption spectral shapes for the smallest cells
a_{micro}	m^{2}mg^{-1}	Phytoplankton absorption spectral shapes for the largest cells
R_{rs}	sr^{-1}	Above-surface remote-sensing reflectance spectra
r_{rs}	sr^{-1}	Below-surface remote-sensing reflectance spectra
$L_u(0^-/0.66)$	Wm^{-2}sr^{-1}	Upwelling radiance just beneath or at 66 cm below the sea surface
$E_d(0^{-/+})$	Wm^{-2}	Downwelling irradiance just below or just above the sea surface.
t		Radiance transmittance of the surface
n		Real index of refraction of water
θ_{s}		Polar direction of the Sun's refracted beam in water

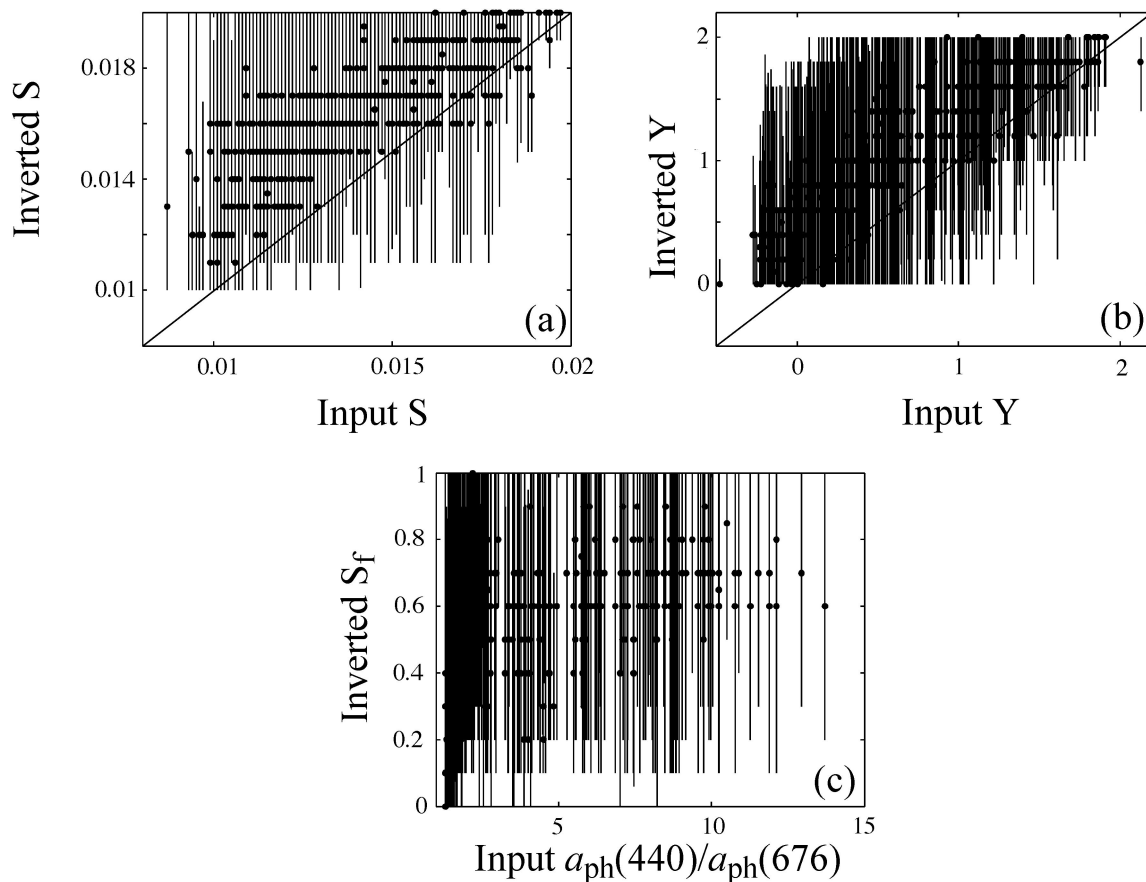*Blank entries denote dimensionless quantities.

Fig. 5. Comparison (a) between the directly calculated and the inverted spectral slope of CDOM+NAP(S), (b) of the spectral slope of particle backscattering, (c) between the size parameter (S_f) for phytoplankton and the ratio of a_{ph} at 440 to 680 nm of the input phytoplankton spectrum. Dots denote the median inverted values, whereas the lines denote the 90% confidence interval in the inverted parameters (based on the statistics of all acceptable solutions).
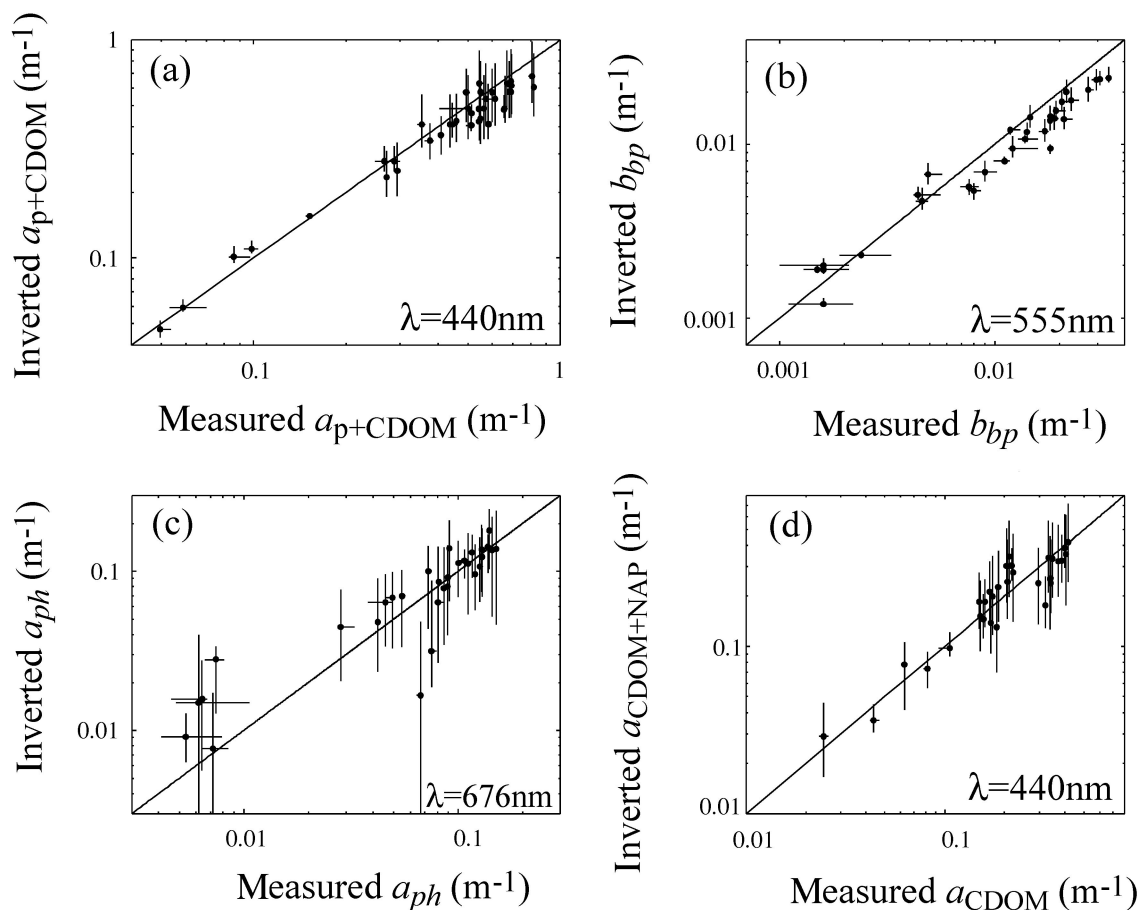
Fig. 6. Comparison for the *in situ* data set between (a) the inverted $a_{\mathrm{p+CDOM}}(440)$ versus ac–9 measured, $a_{\mathrm{p+CDOM}}(440)$, (b) the inverted $b_{bp}(555)$ versus HS6-measured $b_{bp}(555)$, (c) the inverted $a_{\mathrm{ph}}(676)$ versus $a_{\mathrm{ph}}(676)$ derived from ac-9 measurements, (d) the inverted $a_{\mathrm{CDOM+NAP}}(440)$ versus ac-9-measured $a_{\mathrm{CDOM}}(440)$. Dots denote the median values, whereas the vertical lines denote the 90% confidence interval in the inverted parameters. Horizontal lines denote the distance between maximum and minimum values of the *in situ* measured parameters (when larger than the size of the dot).

sured a_{CDOM} values, as the *in situ* measurement does not include absorption by NAP.

The field data set does not contain phytoplankton absorption. We compute the phytoplankton absorption at 676 nm from the phytoplankton absorption line height at 676 nm[38]:

$$a_{\mathrm{ph}}(676) = a_{\mathrm{p+CDOM}}(676) - 0.6a_{\mathrm{p+CDOM}}(650). \quad (14)$$

This procedure is designed to remove the contribution of NAP+CDOM absorption from $a_{\mathrm{p+CDOM}}(676)$.

The linear correlation of $a_{\mathrm{ph}}(676)$ is high; $R = 0.9$, and the median relative and absolute difference are 15% and 0.0124 m^{-1}, respectively [(Fig. 6(d)]. Absorption by phytoplankton at 676 nm is found with less than 13% of the points outside the 90% confidence interval.

Because we did not have information on the size of the underlying phytoplankton during the field measurements, we attempted to correlate the phytoplankton size factor S_f with the slope of the particulate beam attenuation for the *in situ* data. The slope of particulate beam attenuation was found to correlate with the particle size distribution.[39] The low

linear correlation ($R = 0.08$) indicate that the relation between the size factor for phytoplankton and the slope of the particulate beam attenuation is not significant.

Comparison of the inverted spectral slope of CDOM+NAP (S) and particulate backscattering (Y) with the calculated values for the measured spectra yield $R = 0.2$ for S and $R = 0.09$ for Y with large inversion uncertainties. Thus, while the amplitudes of the IOPs are retrieved well and within the computed uncertainties, the spectral shape parameters are not retrieved within a useful range (Fig. 7).

4. Conclusions

A novel method to provide uncertainties in inverted parameters obtained from remotely sensed reflectance data was developed. This method was applied to a specific semianalytical inversion scheme to retrieve the particulate backscattering coefficients and the absorption coefficients of phytoplankton pigments and CDOM and NAP, as well as the uncertainties in the inverted parameters. This approach to compute uncertainties is general and can be adapted to all current semiempirical inversion schemes. Such
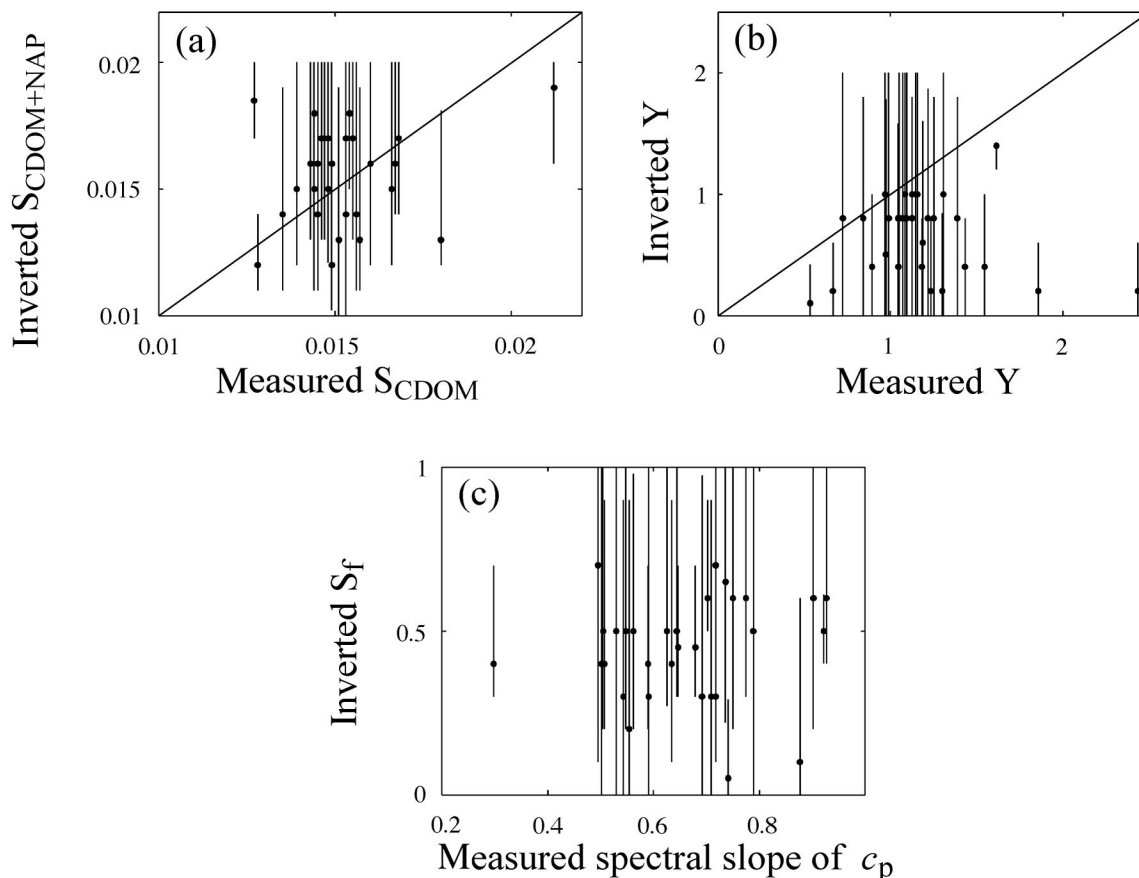
Fig. 7. (a) Comparison between the inverted spectral slope of CDOM and NAP and the calculated spectral slop of CDOM measured with the ac-9. (b) Comparison between the inverted spectral slope of particulate backscattering and the calculated spectral slope of particulate backscattering (Y) based on measurements with the HS-6. (c) Comparison between the phytoplankton size factor S_f and the slope of the particulate beam attenuation for the *in situ* data. Uncertainties in measured spectral slopes were less than 0.002 for S, 0.1 for Y, and 0.1 for the slope of c_p. Dots denote the median values, whereas the lines denote the 90% confidence interval.

adaptation will require a discretization of all shape factors so that a linear system can be solved as presented above.

To test the performance of the algorithm, we applied it to both a simulated and a field data set of hyperspectral remotely sensed reflectance (r_{rs}). The low median absolute differences of inverted IOPs and high linear correlation with input or measured IOPs suggest that the specific scheme used here can extract the absorption and backscattering from r_{rs} successfully in both the simulated and the field data sets.

We concentrated on quantifying uncertainties in the retrieved IOPs because of uncertainties in the values of the radiance measurement, uncertainties in the spectral shape of IOPs and uncertainties in the relation between the r_{rs} and the IOPs. Using both a field and simulated data set, we found that the specific inversion scheme to quantify uncertainties works well: at least 80% of the absorption amplitudes were within the 90% confidence intervals. Separating the component of absorption we find that more of the measurements (or inputs) are outside the uncertainty bound.

The percentage of the backscattering coefficient within the 90% confidence interval was significantly lower ($\sim$50%) compared with the absorption coefficients. This lower percentage may be because backscattering is not necessarily well described by a power law as a function of wavelength, in particular in waters dominated by phytoplankton.[33,40]

Little is known about natural variability of the backscattering spectral slope, Y.[33,34] Comparisons between the inverted and the directly calculated spectral slopes of particle backscattering (Y) based on the simulated data set suggest that the inversion algorithm can provide a reliable Y prediction. The comparison of spectral slopes for the field data, however, does not work well, as predicted uncertainties are too large to be of practical use.

Attempts to link a size factor (S_f) for phytoplankton to a measure of pigment packaging [$a_{ph}(676)/a_{ph}(440)$] or the spectral slope of the particulate beam attenuation were not successful. Inversion uncertainties are large and correlations with related parameters from both simulated and *in situ* data are weak. This failure may be due to our choice of a model for a_{ph} [Eq. 5] not matching well the underlying phytoplankton absorption and the sensitivity of S_f to the uncertainties in our inversion input and procedure, as highlighted by the large uncertainties. For the *in situ*

data set, the lack of correlation with the spectrum of particulate attenuation may be an indication that phytoplankton did not dominate attenuation in these data (though other evidence, namely, the value of the particulate backscattering ratio,[41] suggests they did).

Possible improvements of the specific inversion scheme used here may be the use of a library of phytoplankton absorption rather than an analytical expression,[40] addition of wavelengths in the infrared to better constrain b_{bp},[42] and inclusion of inelastic scattering effects on r_{rs}.[43]

The scheme to obtain the uncertainties presented here relies on solving a linear problem approximately 1000 times for each r_{rs} spectra. Given advances in linear computation techniques, this should not pose a problem for applications with large data sets. It could also be used, for example, on a subset of a satellite image to provide estimates of the uncertainties while taking into account the known spatial decorrelation scales. In addition, the linear scheme used here always finds the one best solution (in a linear least-squares sense[35]), which is not guaranteed with nonlinear inversion schemes used currently in most semianalytical models.[9,10,12,44] In the nonlinear inversion case there is no guarantee of finding the global minimum in the search for a solution, but rather the local minimum near a given initial guess.[35] This local minimum may be the global minimum sought, yet there is no guarantee that it is.

The minimum number of required wavelengths is three, given the nature of the linear problem we are solving (solving for three amplitudes when three shape parameters are assumed). Additional wavelengths provide additional constraints, reducing the uncertainties on both amplitudes and spectral shapes. It should therefore be possible to use the approach outlined here with current multispectral ocean color satellites. In that case, uncertainties in r_{rs} due to atmospheric correction should be added to the uncertainty budgets.

References

1. R. W. Preisendorfer, *Hydrologic Optics,* (U. S. Department of Commerce, U.S. GPO, Washington, D.C.,1976).

2. C. D. Mobley, *Light and Water. Radiative Transfer in Natural Waters* (Academic, San Diego, Calif., 1994).

3. H. R. Gordon, O. B. Brown, and M. M. Jacobs, "Computed relationships between the inherent and apparent optical properties of a flat homogeneous ocean," Appl. Opt. **14,** 417–427 (1975).

4. A. Morel and L. Prieur, "Analysis of variations in ocean color," Limnol. Ocean. **22,** 709–722 (1977).

5. A. Morel, "Available, usable and stored radiant energy in relation to marine photosynthesis," Deep-Sea Res. **25,** 673–688 (1978).

6. D. Stramski, R. A. Reynolds, M. Kahru, and B. G. Mitchell, "Estimation of particulate organic carbon in the ocean from satellite remote sensing," Science **285,** 239–242 (1999).

7. D. A. Siegel, S. Maritorena, D. A. Hansell, and M. Lorenzi-Kayser, "Global distribution and dynamics of colored dissolved and detrital organic materials," J. Geophys. Res. **107,** 10.1029/2001JC000965 (2002).

8. M. J. Behrenfeld, E. Boss, D. A. Siegel, and D. M. Shea, "Carbon-based ocean productivity and phytoplankton physiology from space" Global Biogeochem. Cycles **19,** GB1006, doi: 10.1029/2004GB002299 (2005).

9. C. S. Roesler and M. J. Perry, "*In situ* phytoplankton absorption, fluorescence emission, and particulate backscattering spectra determined from reflectance," J. Geophys. Res. **100,** 13279–13294 (1995).

10. Z. P. Lee, K. L. Carder, T. G. Peacock, C. O. Davis, and J. L. Mueller, "Method to derive ocean absorption coefficients from remote-sensing reflectance," Appl. Opt. **35,** 453–462 (1996).

11. F. E. Hoge and P. E. Lyon, "Satellite retrieval of inherent optical properties by linear matrix inversion of oceanic radiance models: an analysis of model and radiance measurement errors," J. Geophys. Res. **101,** 16631–16648 (1996).

12. A. H. Garver and D. A. Siegel, "Inherent optical property inversion of ocean color spectra and its biogeochemical interpretation. 1. Time series from the Sargasso Sea," J. Geophys, Res. **102,** 18607–18625 (1997).

13. K. L. Carder, F. R. Chen, Z. P. Lee, S. K. Hawes, and D. Kamykowski, "Semianalytic Moderate-Resolution Imaging Spectrometer algorithms for chlorophyll-a and absorption with bio-optical domains based on nitrate-depletion temperatures," J. Geophys, Res. **104,** 5403–5421 (1999).

14. S. Maritorena and D. A. Siegel, "Consistent merging of satellite ocean color data sets using a bio-optical model," Remote Sens. Environ. **94,** 429–440 (2005).

15. Z. P. Lee, http://www.ioccg.org/groups/lee_data.pdf (2004).

16. Z. P. Lee, http://www.ioccg.org/groups/lee.html (2004).

17. Z. P. Lee, http://www.ioccg.org/groups/OCAG_data.html (2204).

18. G. C. Chang, T. D. Dickey, C. D. Mobley, E. Boss, and W. S. Pegau, "Toward closure of upwelling radiance in coastal waters," Appl. Opt. **42,** 1574–1582 (2003).

19. C. D. Mobley, L. K. Sundman, and E. Boss, "Phase function effects on oceanic light fields," Appl. Opt. **41,** 1035–1050 (2002).

20. A. H. Barnard, W. S. Pegau, and J. R. V. Zaneveld, "Global relationships of the inherent optical properties of the oceans," J. Geophys, Res. **103,** 24955–24968 (1998).

21. J. L. Mueller, G. S. Fargion, and C. R. McClain, eds., *Ocean Optics Protocols for Satellite Ocean Color Sensor Validation*, Rev. 4, in Vol. IV: Inherent Optical Properties: Instruments, Characterizations, Field Measurements and Data Analysis Protocols, TM-2003-211621/Rev4-Vol.IV (NASA, 2003), http://www.wetlabs.com/appnotes/Vol%201V%20v4%20final.pdf.

22. H. R. Gordon and O. B. Brown, "The diffuse reflectance of the ocean: some effects of vertical structure," Appl. Opt. **14,** 2892–2895 (1975).

23. C. D. Mobley, "Notes on converting TSRB data to remote-sensing reflectance," Sequoia Scientific, Inc., Bellevue, Wash. (personal communication, 2000).

24. Z. P. Lee, K. L. Carder, and R. A. Arnone, "Deriving inherent optical properties from water color: a multiband quasi-analytical algorithm for optically deep waters," Appl. Opt. **41,** 5755–5772 (2002).

25. H. R. Gordon, O. B. Brown, R. H. Evans, J. W. Brown, R. C.

Smith, K. S. Baker, and D. K. Clark, "A semianalytic radiance model of ocean color," J. Geophys, Res. **93,** 10909–10924 (1988).

26. R. M. Pope and E. S. Fry, "Absorption spectrum (380–700 nm) of pure water. II. Integrating cavity measurements," Appl. Opt. **36,** 8710–8723 (1997).

27. W. S. Pegau, D. Gray, and J. RonaldV. Zaneveld, "Absorption and attenuation of visible and near-infrared light in water: dependence on temperature and salinity," Appl. Opt. **36,** 6035–6046 (1997).

28. A. M. Ciotti, M. R. Lewis, and J. J. Cullen, "Assessment of the relationship between dominant cell size in natural phytoplankton communities and the spectral shape of the absorption coefficient," Limnol. Oceanogr. **47,** 404–417 (2002).

29. C. S. Roesler, M. J. Perry, and K. L. Carder, "Modeling *in situ* phytoplankton absorption from total absorption spectra in productive inland marine waters," Limnol. Oceanogr. **34,** 1501–1523 (1989).

30. D. Stramski, A. Bricaud, and A. Morel, "Modeling the inherent optical properties of the ocean based on the detailed composition of the planktonic community," Appl. Opt. **40,** 2929–2945 (2001).

31. A. Morel, "Optical properties of pure water and pure sea water," in *Optical Aspects of Oceanography*, N. G. Jerlov and E. S. Nielsen, eds. (Academic, New York, 1974), pp. 1–24.

32. E. Boss and W. S. Pegau, "Relationship of light scattering at an angle in the backward direction to the backscattering coefficient," Appl. Opt. **40,** 5503–5507 (2001).

33. D. Stramski, E. Boss, D. Bogucki, and K. J. Voss, "The role of seawater constituents in light backscattering in the ocean," Prog. Oceanogr. **61,** 27–56 (2004).

34. E. Boss, D. Stramski, T. Bergmann, W. S. Pegau, and M. Lewis, "Why should we measure the optical backscattering coefficient?" Oceanography **17,** 44–49 (2004).

35. W. H. Press, B. P. Flannery, S. A. Teukolsky, and W. T. Vetterling, in *Numerical Recipes in FORTRAN: The Art of Scientific Computing*, 2nd ed. (Cambridge U. Press, 1992), pp. 655–675.

36. J. T. O. Kirk, *Light and Photosynthesis in Aquatic Ecosystems* (Cambridge U. Press, Cambridge, U.K.,1994).

37. A. Bricaud and A. Morel, "Light attenuation and scattering by phytoplanktonic cells: a theoretical modeling," Appl. Opt. **25,** 571–580 (1986).

38. R. F. Davis, C. C. Moore, J. R. V. Zaneveld, and J. M. Napp, "Reducing the effects of fouling on chlorophyll estimates derived from long-term deployments of optical instruments," J. Geophys.Res. **102,** 5851–5855 (1997).

39. E. Boss, M. S. Twardowski, and S. Herring, "Shape of the particulate beam attenuation spectrum and its inversion to obtain the shape of the particulate size distribution," Appl. Opt. **40,** 4885–4893 (2001).

40. C. Roesler and E. Boss, "A novel ocean color inversion model: retrieval of beam attenuation and particle size distribution," Geophys. Res. Let. **30,** 10.1029/2002GL016366 (2003).

41. E. Boss, E. W. S. Pegau, M. Lee, M. S. Twardowski, E. Shybanov, G. Korotaev, and F. Baratange, "The particulate backscattering ratio at LEO 15 and its use to study particles composition and distribution," J. Geophys. Res. **109,** C0101410.1029/2002JC001514 (2004).

42. M. Sydor, B. D. Wolz, and A. M. Thralowa, "Spectral analysis of bulk reflectance from coastal waters: deconvolution of diffuse spectra due to scattering and absorption by coastal water," J. Coast. Res. **18,** 352–361 (2002).

43. D. Pozdnyakov and H. Grassl, "*Colour of Inland and Coastal Waters*," (Springer, Chichester, 2003).

44. S. Maritorena, D. A. Siegel, and A. R. Peterson, "Optimization of a semianalytical ocean color model for global-scale applications," Appl. Opt. **41,** 2705–2714 (2002).